Journal Homepage: -www.journalijar.com
INTERNATIONAL JOURNAL OF ADVANCED RESEARCH (IJAR)
Article DOI:10.21474/IJAR01/1664
DOI URL: http://dx.doi.org/10.21474/IJAR01/1664
ISSN NO. 2320-5407

RESEARCH ARTICLE

EFFECT OF Mn DOPING ON STRUCTURAL AND DIELECTRIC PROPERTIES OF $GdFeO_3$.

Ali O. A. Keelani and Shahid Husain*.
Department of Physics, Aligarh Muslim University, Aligarh-202002, India.

Manuscript Info

Manuscript History

Received: 12 July 2016
Final Accepted: 22 August 2016
Published: September 2016

Key words:-
X-ray diffraction (XRD), Williamson-Hall analysis, Universal dielectric response

Abstract

We have synthesized $GdFe_{1-x}Mn_xO_3$ (x=0.0, 0.1, 0.2 and 0.3) by solid state reaction route in order to understand their structural and dielectric properties. X-ray diffraction (XRD) patterns confirm single phase nature and the orthorhombic crystal symmetry of our samples. The lattice parameters are determined from the PowderX software, and are found to decrease with increase in Mn concentration. The most intense peak shifts towards lower 2θ values with increase in Mn concentration indicating the development of strain in the crystal structure. Williamson-Hall-plots of $GdFe_{1-x}Mn_xO_3$(GFMO) are used to investigate physical parameters such as strain, stress, and energy density using different models namely, uniform deformation model (UDM), uniform deformation stress model (UDSM) and uniform deformation energy density model (UDEDM). The strain, stress, energy density and crystallite size increase as the concentration of Mn increases. The value of dielectric constant (ε') is found to decrease with the increase in frequency while it enhanced with increase in Mn concentration. The log (f × ε') versus log (f) graphs have been plotted to verify the universal dielectric response (UDR) behavior. All the samples follow UDR model almost in the whole range of measured frequencies.

Introduction:-

Rare earth orthoferrites of the chemical formula $RFeO_3$ (where R is the rare earth ion) show diverse magnetic and electrical properties due to interaction of R^{3+} and Fe^{3+} ions. These materials are important candidate for several applications due to possibility of ultrafast control of spins [1-8]. This property makes these orthoferrites as potential materials for the spintronics devices. $GdFeO_3$ is one of the important members of rare earth orthoferrites that crystallizes in orthorhombic distorted perovskite phase, with Gd^{3+} ions at the corners of the cube and Fe^{3+}ions at the body center positions [2, 3].The magnetic sub-structure is composed of two interpenetrating pseudo-cubic face-centred sub-lattices of Fe^{3+} ions, where each Fe^{3+} ion is surrounded by six O^{2-} ions, forming FeO_6 octahedron. The doping at Fe site produces distortion in the FeO_6 octahedron and hence the strain in the lattice. This lattice strain plays the pivotal role in governing the properties of $GdFeO_3$. In the literature we do not find any study on the determination of lattice strain and stress produced in the $GdFeO_3$ on doping at Fe site. Moreover, $GdFeO_3$ is typically used for terahertz sensor, frequency tunable terahertz lasers, and magneto-optical data storage [9, 10]. In view of above we have synthesized $GdFe_{1-x}Mn_xO_3$ (x=0.0, 0.10, 0.20, and 0.30) and studied their structural, morphological and dielectric properties.

Corresponding Author:-Shahid Husain.
Address:-Department of Physics, Aligarh Muslim University, Aligarh-202002, India.

Experimental:-

We have employed the standard solid state reaction route to prepared nano-crystalline samples of $GdFe_{1-x}Mn_xO_3$(x=0.0, 0.1, 0.2, and 0.3). The stoichiometric amounts of high purity $MnCO_3$, Fe_2O_3, and Gd_2O_3, powders are mixed together thoroughly and preheated at 1000 $^{\circ}$C for 20 hours. After first heat treatment, these samples are ground again and sintered at 1150 $^{\circ}$C, with two intermediate grindings. Finally, the mixtures are pressed into pellets and followed by sintering in air at 1200 $^{\circ}$C and cooled down to room temperature slowly at the rate of 5°C/min. The crystal structure of the sample is analyzed by x-ray diffraction (XRD) using Shimadzu LabX XRD-6100 advance diffractometer (Cu-K_α radiation) at room temperature in the 2θ range of 20°-80°. The dielectric properties were measured using Agilent 6300A precision LCR meter (Accuracy of set frequency ±0.005% with Frequency step size: ≤1mHz) as a function of frequency of the applied ac field in the range of 75 KHz to 5 MHz.

Results and Discussion:-

Structural Analysis:-

X-ray powder diffraction (XRD) patterns for $GdFe_{1-x}Mn_xO_3$ (0< x <0.3) recorded at room temperature show that all the samples are in single phase with no detectable secondary phases as shown in Fig. 1. Further, these samples have orthorhombic crystal symmetry with Pbnm space group. The lattice parameters are determined using PowderX software and crystallite sizes are calculated using Sherrer equation. Since ionic radii of Fe^{3+} is 0.067 nm and that of Mn^{3+} is 0.064nm therefore it is obvious that lattice parameters and unit cell volume would decrease with the increase in Mn concentration as shown in Fig. 2. The crystallite sizes are found to lie in the range of 34 to 37 nm. The lattice parameters and crystallites sizes for all the samples are tabulated in Table 1. We believe that introducing Mn at Fe site will cause a distortion in FeO_6 octahedron. Consequently, Mn–O–Mn and Fe-O-Fe bond angles decrease with the increase in Mn concentration while Fe-O and Mn-O bond length increases as displayed in Table 1. Further, the distortion of FeO_6 octahedron induces strain in the lattice. That is reflected in the shift of the most intense peak towards higher value of 2θ with the increase in Mn doping (x=0.10 and 0.20) but further doping (x=0.30) shifts the peak towards lower value as shown in Fig. 3.

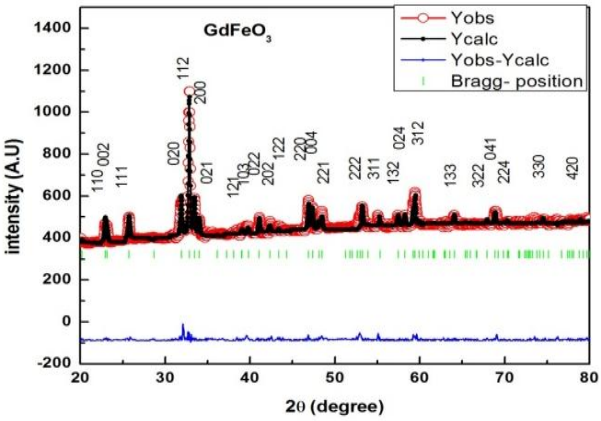

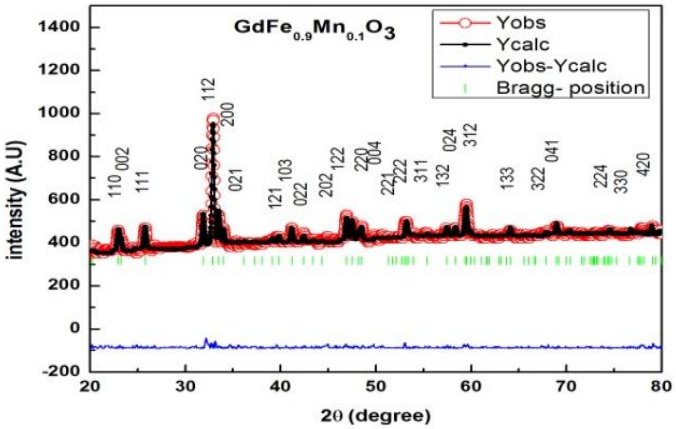

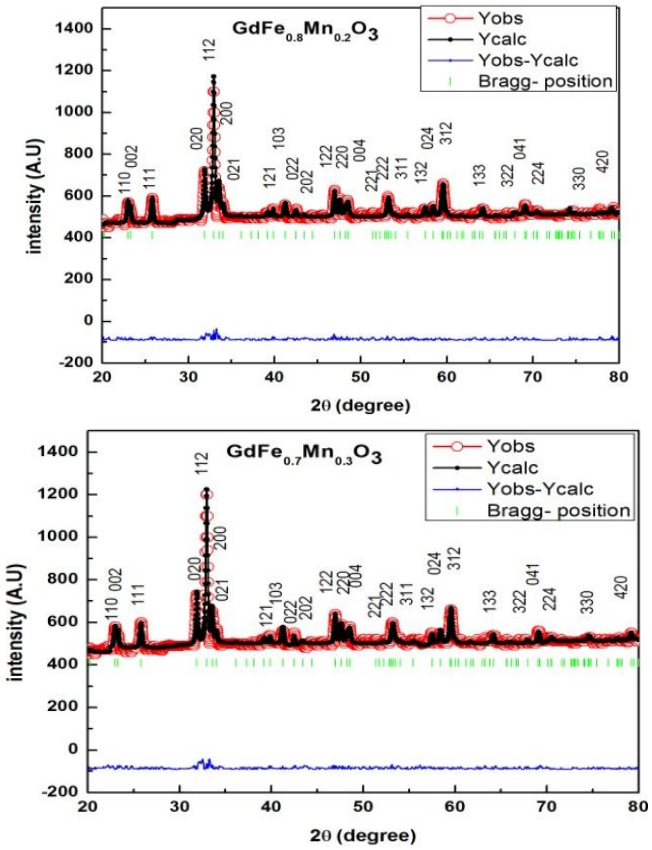

Fig 1:- X-ray diffraction patterns of $GdFe_{1-x}Mn_xO_3$(x=0.0, 0.1, 0.2 and 0.3).The experimental data points are indicated by red circles, and the calculated profile by black solid circles. The lowest curve shows the differences between the experimental and the calculated data. The vertical bars indicate the expected reflection positions for orthorhombic structure.

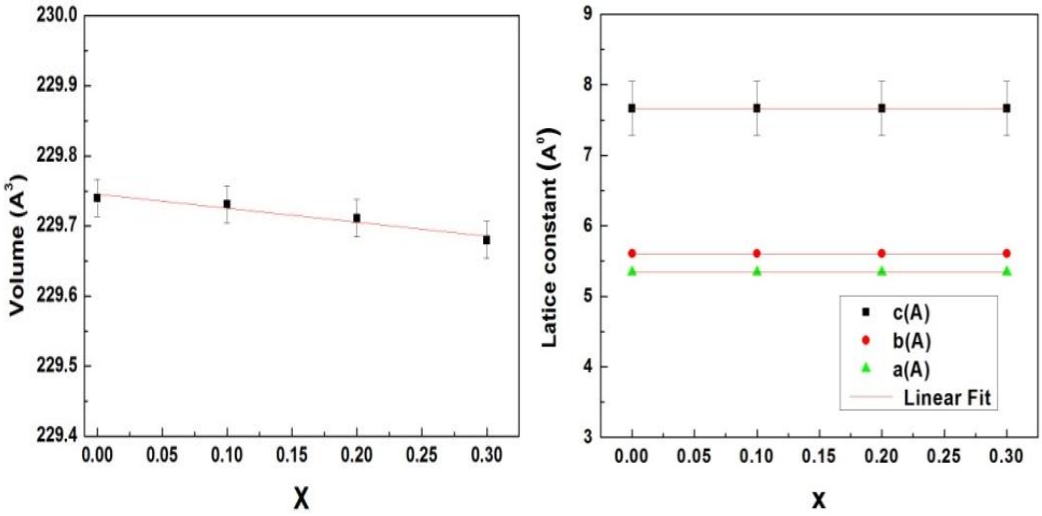

Fig 2:- Effect of Mn doping (x) on volume of the unit cell volume and lattice constants.

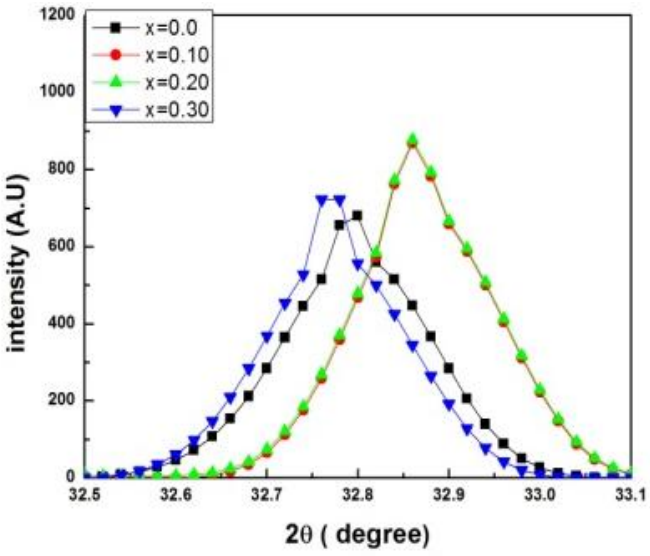

Fig 3:- Shift of most intense peak as Mn concentration.

Table1:-Refined structural parameters of $GdFe_{1-x}Mn_xO_3$ (x = 0.0, 0.1, 0.2 and 0.3) at room temperature.

Parameter	x = 0.0	x = 0.1	x = 0.2	x = 0.3
a (Å)	5.3465±0.0077	5.3460±0.0077	5.3457±0.0077	5.3455±0.0077
b (Å)	5.6058±0.0080	5.6064±0.0080	5.6063±0.0080	5.6059±0.0080
c (Å)	7.6653±0.0110	7.6649±0.0110	7.6648±0.0110	7.6646±0.0110
V $(Å)^3$	229.74	229.73	229.71	229.68
Crystallite size (nm)	34.11	34.11	37.22	37.22
Fe–O (Å)	2.006	2.061	2.138	2.143
Gd–O1 (Å)	2.202	2.176	1.953	1.8929
Gd–O2 (Å)	2.494	2.474	2.309	2.430
Mn-O (Å)	-	2.0610	2.1382	2.1434
(Mn-O-Mn) (θ)	-	136.2	126.4	125.9
(Fe-O-Fe) (θ)	145.6	136.2	126.4	125.9
R_p (%)	16.3	15.8	14.8	13.2
R_{wp}	12.4	14.3	13.6	14.7
R_{exp}	10.6	12.9	12.8	11.7
χ^2	1.37	1.23	1.13	1.58

Williamson-Hall-analysis:-

Uniform deformation model (UDM)

The significance of the broadening of peaks indicates grain refinement along with the strain associated with the samples. The instrumental broadening (β_{hkl}) was corrected, corresponding to each diffraction peak using the relation [11]:

$$\beta_{hkl} = [(\beta_{hkl})^2_{measured} - (\beta_{hkl})^2_{instrumental}]^{\frac{1}{2}} \quad (1)$$

The average crystallite size was calculated using Scherrer equation:

$$D = \frac{K\lambda}{\beta hkl cos\theta} \quad (2)$$

where D represents crystallite size, K is the shape factor (0.89), and λ represents wavelength of Cu-K_α radiation.
The strain induced in samples due to crystal imperfection and distortion was calculated using the formula:

$$\varepsilon = \frac{\beta_{hkl}}{4\ tan\theta} \quad (3)$$

From equations (2) and (3), it is evident that the crystallite size and strain varies as 1/cosθ and tanθ. Assuming that the crystallite size and strain contributions to line broadening are independent to each other and both have a Cauchy-like profile, the observed line width is simply the sum of equations (2) and (3).

$$\beta_{hkl} = \frac{K\lambda}{D\cos\theta} + 4\varepsilon\tan\theta \quad (4)$$

On rearranging the above equation we get,

$$\beta_{hkl}cos\theta = \frac{K\lambda}{D} + 4\,\varepsilon sin\theta \quad (5)$$

The above equation is Williamson-Hall equation under the uniform deformation model. The strain is assumed to be uniform in all crystallographic directions, thus considering the isotropic nature of the crystal, where the material properties are independent of the direction along which they are measured. The full width at half maximum (FWHM) (β) and the angle θ for a particular peak are determined from XRD patterns. The βcos(θ) versus 4sin(θ) graphs are plotted and fitted linearly to estimate crystallite size and strain for different Mn concentrations as shown in Fig. 4. These parameters are tabulated in Table 2.

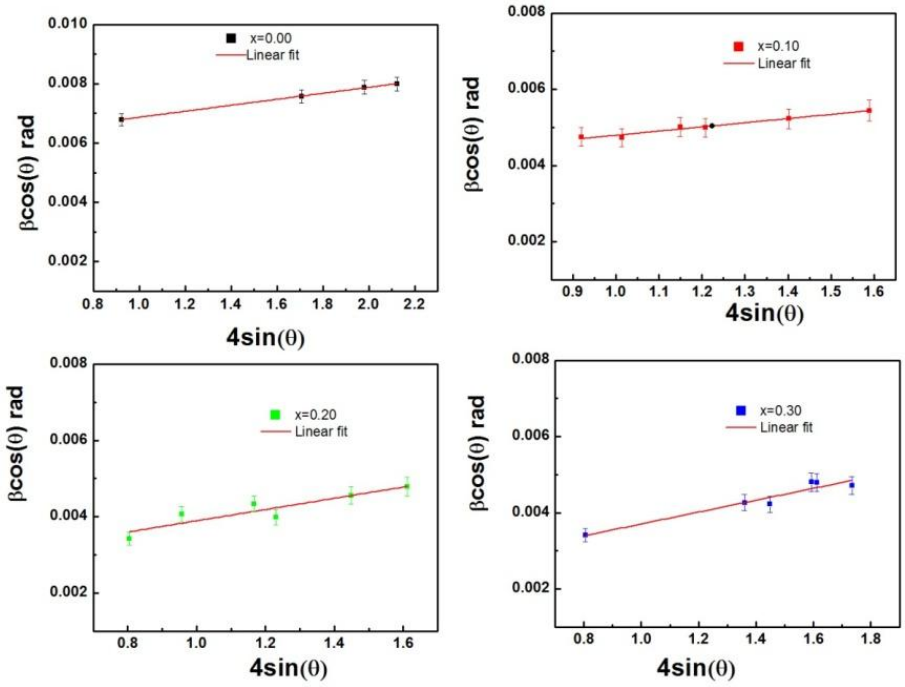

Fig 4:-βcos(θ) versus 4sin(θ) plots with linear fit of $GdFe_{1-x}Mn_xO_3$(x=0.0, 0.1, 0.2 & 0.3).

Table2:-Crystallite size and strain for $GdFe_{1-x}Mn_xO_3$ (x=0, 0.10, 0.20, 0.30) as estimated using Williamson-Hall plots under UDM model.

Composition	Intercept (βcos(θ))	Slope	Crystallite Size (nm)	Strain
$GdFeO_3$	$3.88 \times 10^{-3} \mp 4.07 \times 10^{-5}$	$1.01 \times 10^{-7} \mp 2.33 \times 10^{-9}$	35.3	$1.01 \times 10^{-7} \mp 2.33 \times 10^{-9}$
$GdMn_{0.1}Fe_{0.9}O_3$	$3.70 \times 10^{-3} \mp 1.29 \times 10^{-4}$	$1.20 \times 10^{-7} \mp 1.05 \times 10^{-8}$	37.0	$1.20 \times 10^{-7} \mp 1.05 \times 10^{-8}$
$GdMn_{0.2}Fe_{0.8}O_3$	$3.68 \times 10^{-3} \mp 4.05 \times 10^{-4}$	$1.48 \times 10^{-7} \mp 3.28 \times 10^{-8}$	37.2	$1.48 \times 10^{-7} \mp 3.28 \times 10^{-8}$
$GdMn_{0.3}Fe_{0.7}O_3$	$3.36 \times 10^{-3} \mp 5.15 \times 10^{-4}$	$1.56 \times 10^{-7} \mp 2.09 \times 10^{-8}$	40.8	$1.56 \times 10^{-7} \mp 2.09 \times 10^{-8}$

Uniform deformation stress model (UDSM):-

In this model uniform deformation stress and uniform deformation energy density were taken into account assuming the anisotropic nature of Young's modulus of the crystal which is more realistic [12-14]. The generalized Hook's law referred to the strain, keeping only the linear proportionality between the stress and strain, i.e., (σ = Eε). Here,

the stress is proportional to the strain, with the constant of proportionality being the modulus of elasticity or Young's modulus, denoted by E. In this approach, the Williamson-Hall equation is modified by substituting the value of ε in equation 5; we get

$$\beta_{hkl}cos\theta = \frac{K\lambda}{D} + \frac{4\,\sigma sin\theta}{E_{hkl}} \quad (6)$$

E_{hkl} is Young's modulus in the direction perpendicular to the set of the crystal lattice planes (hkl). The uniform stress and crystallite size can be calculated from the slope and intercept of the linear fit of the graph plotted between $4\sin\theta/E_{hkl}$ and $\beta_{hkl}\cos\theta$, as shown in Fig. 5. The strain can be measured if $E_{hkl}$is related to their elastic compliances S_{ij} .The expression for the reciprocal of Young's modulus E in the direction of the unit vector l_i in the orthorhombic crystal symmetry with Pbnm space group is given by [15-17]

$$\frac{1}{E_{hkl}} = l_1^4 S_{11} + 2l_1^2 l_2^2 S_{12} + 2l_1^2 l_3^2 S_{13} + l_2^4 S_{22} + 2l_2^2 l_3^2 S_{23} + l_3^4 S_{33} + l_2^2 l_3^2 S_{44} + l_1^2 l_3^2 S_{55} + l_1^2 l_2^2 S_{66} \quad (7)$$

The angle between two different crystal directions $[h_1k_1l_1]$ and $[h_2k_2l_2]$ for an orthorhombic system is [18]

$$\cos(\varphi) = \frac{a^2h_1h_2 + b^2k_1k_2 + c^2l_1l_2}{\sqrt{(a^2h_1^2 + b^2k_1^2 + c^2l_1^2)(a^2h_2^2 + b^2k_2^2 + c^2l_2^2)}} \quad (8)$$

By taking $l_1$crystal direction between [100] and [hkl], $l_2$crystal direction between [010] and [hkl], and $l_3$crystal direction between [001] and [hkl], and using equations (7) and (8) we find,

$$\frac{1}{E_{hkl}} = [(a^4h^4S_{11} + 2a^2h^2b^2k^2S_{12} + 2a^2h^2c^2l^2S_{13} + b^4k^4S_{22} + 2b^2k^2c^2l^2S_{23} + c^4l^4S_{33} + b^2k^2c^2l^2S_{44} + a^2h^2c^2l^2S_{55} + a^2h^2b^2k^2S_{66})/(a^2h^2 + b^2k^2 + c^2l^2)^2] \quad (9)$$

In a perovskite type of orthorhombic crystal systems, S_{ij} are obtained with all the ions relaxed in the cell. The calculated values are 272.0, 263.8, 323.2, 73.0, 67.4, 94.3, 162.9, 130.5, and 110.0 GPa for S_{11}, S_{22}, S_{33}, S_{44}, S_{55}, S_{66}, S_{12}, S_{13}, and S_{23}, respectively [19].

We have found that crystallite size and stress increase with the increase in Mn concentrations as tabulated in Table 3. Strain versus stress plot also shows an increasing trend with the increase in Mn concentration as shown in Fig. 6.

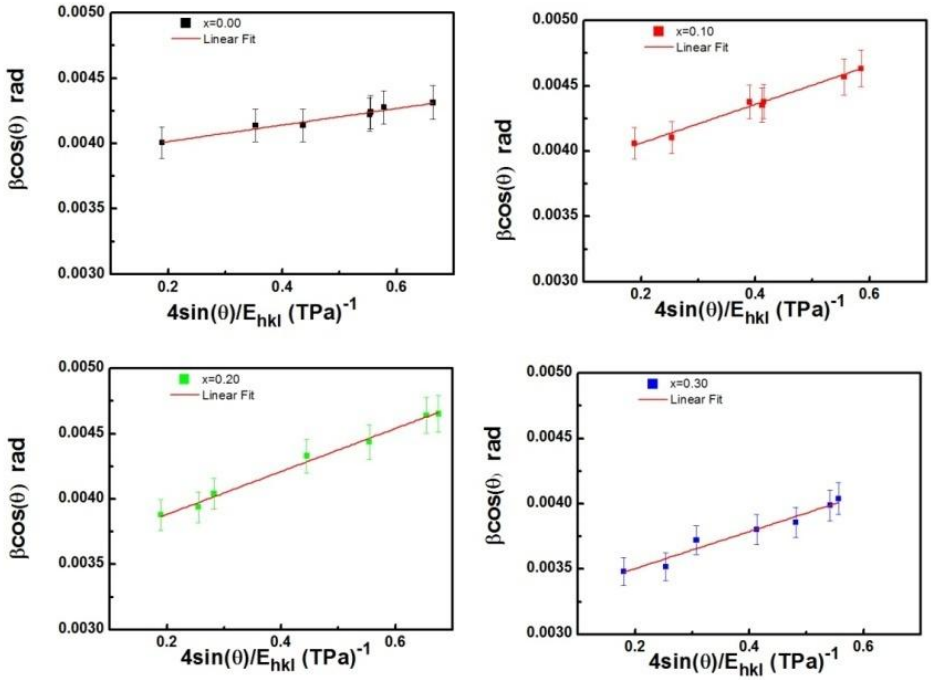

Fig 5:-βcos(θ) versus $4\sin(\theta)/E_{hkl}$plots with linear fit of $GdFe_{1-x}Mn_xO_3$(x=0.0, 0.1, 0.2 and 0.3).

Table 3:-Crystallite size and stress of $GdFe_{1-x}Mn_xO_3$ (x=0, 0.10, 0.20, 0.30) as estimated using Williamson Hall plot under UDSM model.

Composition	Intercept (βcos(θ))	Slope	Crystallite Size (nm)	σ (MPa)
$GdFeO_3$	3.89×10^{-3}	1.42×10^{-4}	35.23	142.25
$GdMn_{0.1}Fe_{0.9}O_3$	3.77×10^{-3}	1.46×10^{-4}	36.35	146.68
$GdMn_{0.2}Fe_{0.8}O_3$	3.55×10^{-3}	1.52×10^{-4}	38.60	152.12
$GdMn_{0.3}Fe_{0.7}O_3$	3.22×10^{-3}	1.56×10^{-4}	42.56	156.24

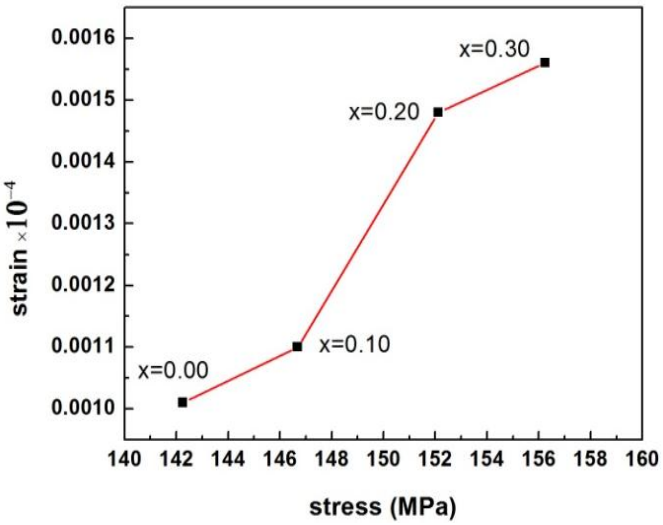

Fig 6:- Strain versus stress plot of $GdFe_{1-x}Mn_xO_3$ (x=0, 0.10, 0.20, 0.30).

Uniform deformation energy density model (UDEDM):-

In equation (5), we have considered the homogeneous isotropic nature of the crystal. However, in many cases, the assumption of homogeneity and isotropy is not fulfilled. Moreover, all the constants of proportionality associated with the stress–strain relation are no longer independent when the strain energy density u is considered. According to Hooke's law, the energy density u (energy per unit volume) as a function of strain is $u = \varepsilon^2 E_{hkl}/2$. Therefore, equation (5) can be modified to the form:

$$\beta_{hkl}cos\theta = \frac{K\lambda}{D} + 4\ sin\theta\left(\frac{2u}{E_{hkl}}\right)^{\frac{1}{2}} \quad (10)$$

where u is the energy density (energy per unit volume)

The uniform deformation energy density can be calculated from the slope of the graph plotted between $\beta_{hkl}\cos\theta$ and $4\sin\theta\ (2/E_{hkl})^{1/2}$. The lattice strain can be calculated by knowing the E_{hkl} values of the sample. W-H equations modified assuming UDEDM and the corresponding plots are shown in Fig. 7. Using equations (6) and (8), the deformation stress and deformation energy density are related as $u = \sigma^2/E_{hkl}$. The estimated value of crystallite size and energy density value are found to increase with the increase in the Mn concentrations.

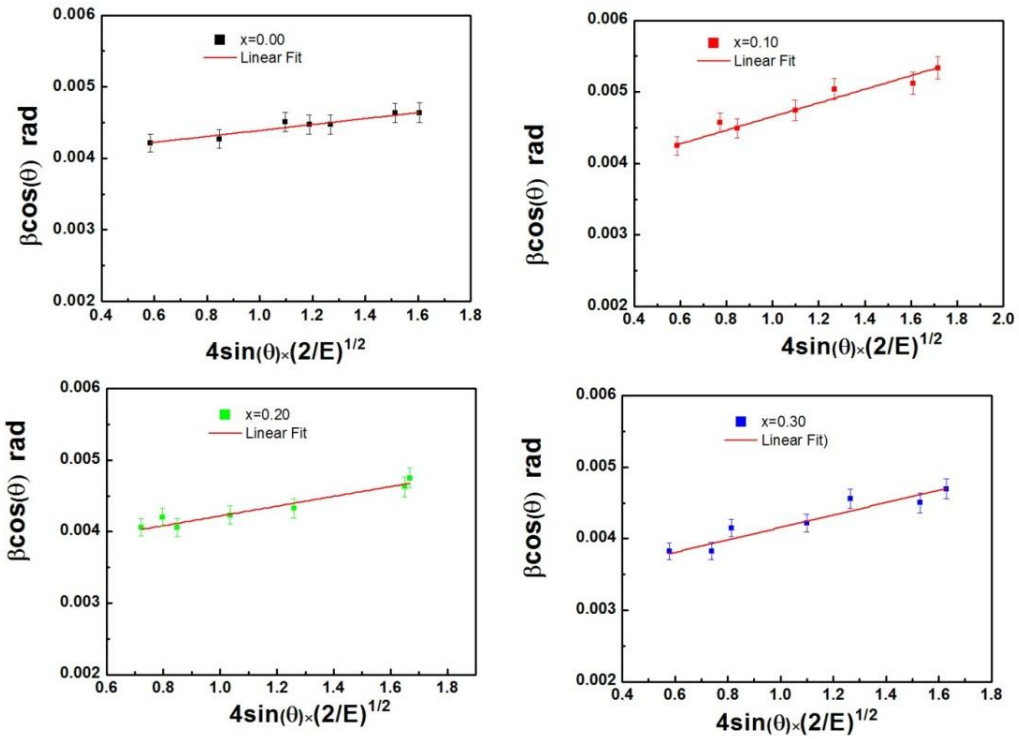

Fig 7:-βcos(θ) versus $4\sin(\theta)(2/E_{hkl})^{1/2}$plots with linear fit for $GdFe_{1-x}Mn_xO_3$(x=0.0, 0.1, 0.2 & 0.3).

Table 4:-Crystallite size and energy density of $GdFe_{1-x}Mn_xO_3$ (x=0, 0.10, 0.20, 0.30) as estimated using Williamson Hall plot under UDSEM model

Composition	Intercept (βcos(θ))	Slope	Crystallite Size (nm)	Energy density (u) (kJm^{-3})
$GdFeO_3$	3.97×10^{-3}	4.16×10^{-04}	34.52	173.25
$GdMn_{0.1}Fe_{0.9}O_3$	3.70×10^{-3}	4.32×10^{-04}	37.04	186.92
$GdMn_{0.2}Fe_{0.8}O_3$	3.53×10^{-3}	4.41×10^{-04}	38.82	194.56
$GdMn_{0.3}Fe_{0.7}O_3$	3.29×10^{-3}	4.48×10^{-04}	41.65	200.90

Dielectric properties:-

We have measured the dielectric constant of $GdFe_{1-x}Mn_xO_3$ ($0 < x < 0.3$) as a function of frequency in the range of 75 kHz to 5 MHz at room temperature as shown in Fig. 8. It is evident from these plots that real part of dielectric constant (ε) decreases with the increase in frequency. The parent system, $GdFeO_3$, shows relatively lower value of ε but its value increases with the increase in Mn concentration. The low value of dielectric constant is attributed to nano-crystalline nature of our samples. As smaller grains contain large surface boundaries and are regions of high resistance. This reduces the interfacial polarization and hence the dielectric constant is found to be smaller than those reported for bulk materials [20]. But as the crystallite size increases with the increase in Mn concentration, dielectric constant also exhibits an increase. Alternatively, A chemical pressure is created in the $GdFeO_3$ lattice on doping with Mn^{3+}, a Jahn-Teller ion. This may result in conversion of Mn^{3+} to Mn^{4+} ion. In order to preserve charge neutrality in the system Fe^{3+} ions convert into Fe^{2+} ions in proportionate amount. It employs that Mn doping give rise to formation of Fe^{2+} ions on the octahedral sites. Consequently, electron hopping starts between Fe^{3+} and Fe^{2+} ions. Therefore, polarization increases and hence the dielectric constant also increases. The decrease of dielectric constant at higher frequency can be explained on the basis of space charge polarization model of Maxwell [21] and is also in agreement with the Koop's phenomenological theory [22]. The decrease of dielectric constant at higher frequency can be explained on the basis that the solid is assumed as composed of well conducting grains separated by poorly conducting grain boundaries. The electrons reach the grain boundary through hopping and if the resistance of the grain boundary is high enough, electrons pile up at the grain boundaries and produce polarization. However,

as the frequency of the applied field is increased beyond a certain value, the electrons cannot follow the alternating field. This decreases the probability of electrons reaching the grain boundary and as a result polarization decreases.This behavior is consistent with other orthoferrites [23, 24].

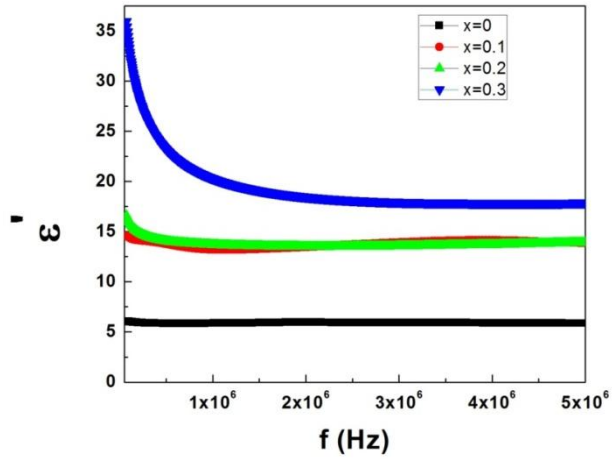

Fig 8:- Real part of dielectric constant as a function of frequency for $GdFe_{1-x}Mn_xO_3$(x=0.0, 0.1, 0.2 and 0.3).

In order to understand the nature of the dielectric response of the samples, the frequency dependent data at room temperature was analyzed in the light of universal dielectric response (UDR) model [25].According to this model, localized charge carriers hopping between spatially fluctuating lattice potentials not only produce the conductivity but may give rise to the dipolar effects. To verify this behavior, we have plotted $\log(\varepsilon' \times f)$as a function of log (f)as shown in Fig. 9. The plots should show a linear behavior and we have found the best linear fit for the host $GdFeO_3$ in the whole frequency range and for the x=0.30 sample the linear behavior deviates slightly at lower frequencies. Therefore, we conclude that UDR phenomenon is responsible for dielectric response in these samples in the whole frequency range except for x=0.30 that too at lower frequencies.

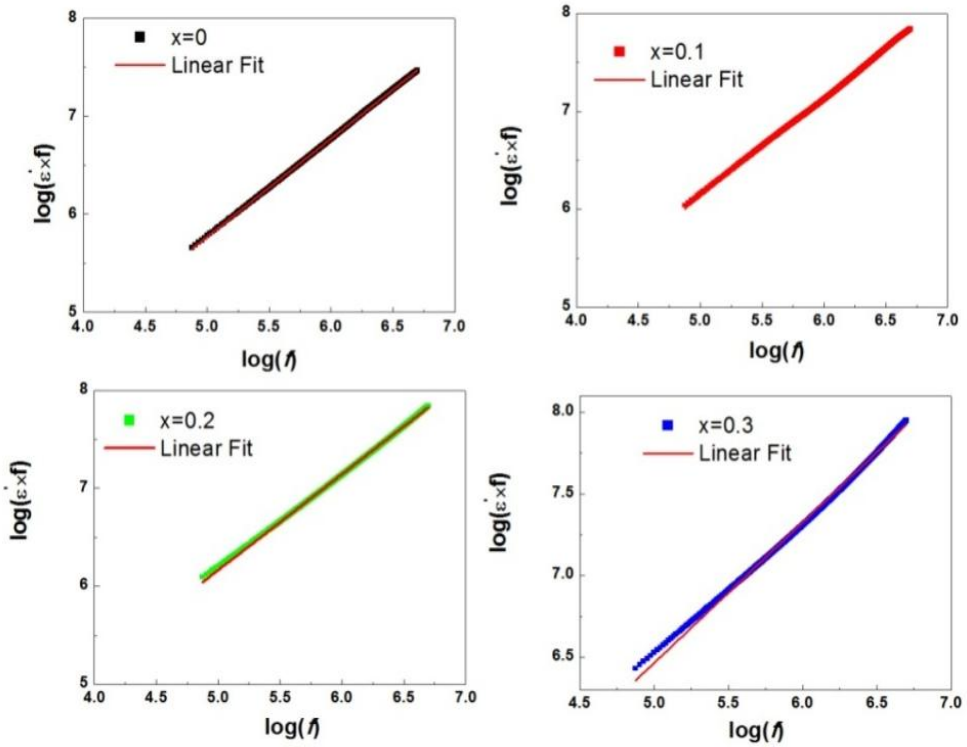

Fig 9:- Plots of $\log(\varepsilon' \times f)$ versus log(f)with linear fit for $GdFe_{1-x}Mn_xO_3$(x=0.0, 0.10, 0.20 and 0.03).

Conclusions:-

We have synthesized nano-crystalline samples of $GdMn_xFe_{1-x}O_3$ (x=0, 0.10, 0.20 and 0.30) by solid state reaction route and studied their structural, morphological and dielectric properties. X-ray diffraction (XRD) patterns confirm single phase nature with orthorhombic Pbnm symmetry. The lattice parameter determined from the refinement program and unit cell volume decrease with increase in Mn content. The most intense peak shifts with the increase in Mn content, indicating the development of strain in the crystal structure. All relevant physical parameters such as strain, stress, and energy density values were also calculated using W-H analysis with different models, viz. uniform deformation model (UDM), uniform deformation stress model (UDSM) and uniform deformation energy density model (UDEDM). We have found that as the concentration of Mn increases the strain, stress, energy density and size of particle increase for all models. Dielectric responses of studied systems have been analyzed in the light of "universal dielectric response (UDR)" model. We have found that all the samples follow the linear behavior in whole frequency range. It means that UDR phenomenon is responsible for dielectric response of these samples at all frequency regimes. The value of dielectric constant (ε') shows increase with increase in Mn concentrations. The observed higher values of dielectric constant reveal that there is hopping between Mn^{+3} to Mn^{+4} and Fe^{+3} to Fe^{+2} at the octahedral sites of the system.

References:-

1. Z. Jin, Z. Mics, G. Ma, Z. Cheng, M. Bonn, D. Turchinovich; Phys. Rev. B., 87 (2013) p. 094422.
2. M.A. Gilleo; J. Chem. Phys., 24 (1956) p.6.
3. Y. Tokunaga, N. Farukawa, H. Sakgi, Y. Taguchi, T. Arima, Y. Tokara; Nat. Mater., 8 (2009) p. 558.
4. J. Shah, R. Kotnala; Scr. Mater., 67 (2012) p. 316.
5. R.L. White; J. Appl. Phys., 40 (1969) p. 106.
6. T. Moriya; Phys. Rev., 120 (1960) p. 91.
7. P.W. Anderson; Phys. Rev., 79 (1950) p. 350.
8. K.C. Nowack, F.H.L. Koppens, Yu.V. Nazarov, L.M.K. Vandersypen; Science, 318 (2007) p. 143. Bashir, M. Ikram, Ravi Kumar, P.N. Lisboa-Fillho; J. Alloys Comp., 521 (2012) p. 183.
9. F. Soderlind, L. Selega, P. Nordblad, K. Uvdal, P.O. Ka; J. Sol–Gel. Sci. Technol., 49 (2009) p. 253.
10. Y.T. Prabhu, K. V. Rao, V.S. S. Kumar, B. S. Kumari; World J. Nanoscience and Engg.,4 (2014) p.21.
11. C. Suryanarayana , M. Grant Norton: X-ray Diffraction: A Practical Approach. Springer, New York (1998).
12. S. Adachi : Handbook on Physical Properties of Semiconductors. Springer, New York (2004).
13. Jian-Min Zhang, Yan Zhang, Ke-Wei Xu, Vincent Ji; Sol. State Commun. 139 (2006) p.87.
14. J.F. Nye, Physical Properties of Crystals: Their Representation by Tensors and Matrices, Oxford Universit Press, Great Britain (1957).
15. Li Shina ,JuXin, Wan Chubin; Computational Materials Science 81 (2014) p.378.
16. M. A. Wahab, Solid State Physics: Structural Properties of Materials; ISBN 978-81-7319-603-4 2nd Edn. Ne Delhi, India (2014) p.23.
17. N. Miao, N.C. Bristowe, Bin Xu, M. J. Verstraete, P. Ghosez; J. Phys. Conden. Matt. 26 (2014) p.035401.
18. R. Hill; Proc. Phys. Soc. London, 65 (1952) p.349.
19. P. Kaur, K. K. Sharma, RabiaPandit, Ravi Kumar, R. Kotnala, Jyoti Shah; J. Appl. Phys.,115 (2014) p.224102.
20. J. C. Maxwell, Electricity and Magnetism (Oxford University Press, New York, 1973).
21. C. G. Koops, Phys. Rev. 83 (1951) p.121.
22. Ahmad, M. J. Akhtar, M. Younas, M. Siddique, and M. M. Hasan, J. Appl. Phys. 112, (2012) p.074105.
23. M. Bhat, B. Kaur, R. Kumar, S. K. Khosa, K. K. Bamzai, P. N. Kotru, and B. M. Wanklyn, Nucl. Instrum. Methods Phys. Res. B 245, (2006) p.480.
24. A.K. Jonscher, J. Phys. D: Appl. Phys. 32 (1999) R57.